WM'02 Conference, February 24–28, 2002, Tucson, AZ

Abstract #327

TSPA MODEL FOR THE YUCCA MOUNTAIN UNSATURATED ZONE

Michael L. Wilson and Clifford K. Ho
Sandia National Laboratories
P.O. Box 5800, Albuquerque, NM 87185

ABSTRACT

Yucca Mountain, Nevada, is being considered as a potential site for a repository for spent nuclear fuel and high-level radioactive waste. Total-system performance-assessment (TSPA) calculations are performed to evaluate the safety of the site. Such calculations require submodels for all important engineered and natural components of the disposal system. There are five submodels related to the unsaturated zone: climate, infiltration, mountain-scale flow of water, seepage into emplacement drifts, and radionuclide transport. For each of these areas, models have been developed and implemented for use in TSPA. The climate model is very simple (a set of climate states have been deduced from paleoclimate data, and the times when climate changes occur in the future have been estimated), but the other four models make use of complex process models involving time-consuming computer runs. An important goal is to evaluate the impact of uncertainties (e.g., incomplete knowledge of the site) on the estimates of potential repository performance, so particular attention is given to the key uncertainties for each area. Uncertainties in climate, infiltration, and mountain-scale flow are represented in TSPA simulations by means of discrete high, medium, and low cases. Uncertainties in seepage and radionuclide transport are represented by means of continuous probability distributions for several key parameters.

INTRODUCTION

The unsaturated zone (UZ) at Yucca Mountain, Nevada, is being considered as the host rock for a potential repository for disposal of spent nuclear fuel and high-level radioactive waste. Water flow in the UZ at Yucca Mountain plays an important role in potential repository performance. Water seeping into waste-emplacement drifts and dripping onto waste packages can accelerate radionuclide mobilization and release. In addition, the UZ acts as the first natural barrier to radionuclides that escape from the potential repository by delaying radionuclide movement. If the delay is long enough that a given radionuclide decays significantly (i.e., if the transport time is large compared to the radionuclide half-life), then the UZ can have a large effect on decreasing the dose from that radionuclide before it reaches the biosphere. TSPA calculations are used to estimate this dose.

TSPA calculations require submodels for all important engineered and natural components of the disposal system. This paper discusses the following five TSPA submodels related to the unsaturated zone: climate, infiltration, mountain-scale flow of water, seepage into emplacement drifts, and radionuclide transport. More-detailed information on these topics, including full description and justification of the models and data, can be found in the *Unsaturated Zone Flow and Transport Model Process Model Report* (1), *Total System Performance Assessment for the Site Recommendation* (2), and additional reports cited therein. In addition, some more-recent work is documented in the *Supplemental Science and Performance Analyses* (3, 4).

CLIMATE

Conceptual Model

Climate refers to the meteorological conditions that characteristically prevail in a particular region. Climate conditions at Yucca Mountain are needed to determine the hydrology within and around Yucca Mountain. In particular, temperature and precipitation are important inputs to the infiltration model.

The climate in the Yucca Mountain region is presently warm and semiarid. However, past climates have exhibited a great deal of variability, alternating between glacial and interglacial periods. During glacial climates, glaciers did not reach Yucca Mountain, but temperatures were lower and precipitation was higher, resulting in greater effective moisture relative to today.

In the conceptual model for future climate at Yucca Mountain, the climate is approximated by a sequence of discrete climate states. The bases for this approach are as follows (1, Section 3.5.1.2):

- Climate is cyclical, with an approximate period of 400,000 years, and this pattern is expected to continue into the future. (Climate is not purely cyclical, however, but has a chaotic component superimposed on the basic cyclical behavior.)

- The timing of past (and future) climates is related to the precession of the Earth's rotational axis (i.e., how the Earth wobbles like a spinning top) and changes in the Earth's orbital eccentricity (i.e., deviation of the orbit from circularity).

- The characteristics of past climates and the sequence of those climates are related. Thus, the analysis can focus on a particular climate sequence and need not take the conservative approach of using the climates that generate the highest infiltration.

- Long-term, Earth-based, climate-forcing processes, such as tectonics, have remained relatively constant over the past 500,000 years or so and should remain so for the period of greatest interest for performance assessment. This is important to climate forecasting because such forcing processes can change climate in noncyclic ways, invalidating the other bases listed above. The effects of such noncyclic forcing processes make climate projections less reliable over longer time periods.

Implementation in the TSPA

The timing and properties of the climate states were derived primarily from the microfossil record of cores drilled at Owens Lake, California (roughly 160 km to the west of Yucca Mountain). The timing of past climates is based on estimates of the rate at which sediment accumulated in the lake bed over time and comparison with the chronology that has been published for calcite deposition at Devils Hole, Nevada (about 50 km southeast of Yucca Mountain). The properties of the past climates (e.g., precipitation and temperature) are based on detailed examination of the Owens Lake cores, in particular for the abundances of various species of ostracode (small freshwater crustaceans) through time. The environmental tolerances

of ostracode species provide a way to estimate the relative water temperature and salinity, thus providing a proxy for climate variations through time (1, Section 3.5.1.3).

The 10,000-year regulatory period has been divided into three climate regimes: modern (present-day), monsoon, and glacial-transition (also called intermediate). Present-day analogs were chosen to represent the future climates; that is, locations that currently have climatic conditions analogous to those deduced for the past climates. Note that the climate discussions in the Process Model Report (1) and in the associated climate report (5) were limited to 10,000 years in the future. The TSPA base case for the site recommendation did not have a detailed climate definition for the period after 10,000 years; the glacial-transition climate was simply extended indefinitely. The climate definition was later extended to 1 million years. The extended sequence cycles between interglacial climates (like the present-day climate), intermediate climates, and glacial climates (2, Section 3.2.5; 3, Section 3.3.1.5).

Treatment of Uncertainty and Variability

Since climate is a large-scale phenomenon, no spatial variability of climate is included in the Yucca Mountain TSPA model. Temporal variability is included as a sequence of climate states, as described above. To capture uncertainty, upper-bound and lower-bound climate analogs were chosen for each climate state, with the upper bound representing wetter conditions and the lower bound representing drier conditions. The TSPA model does not include uncertainty in climate durations.

Results and Interpretation

The climate analogs used for each climate state are summarized in Table I. Multiple analog sites were chosen to represent the future-climate bounds in order to minimize the influence of local meteorological phenomena (1, Section 3.5.1.4).

The climate for the TSPA base case consists of three periods: 600 years with present-day climate, followed by 1,400 years of a monsoon climate, and then a glacial-transition climate for the remainder of the model period. When the extended climate sequence is used, the first glacial climate starts at 38,000 years. The glacial climates are 8,000 to 40,000 years in duration and recur approximately every 90,000 years, on average (2, Table 3.2-4). The intermediate climate occurs approximately 80 percent of the time. The monsoon climate is somewhat warmer than present and with a potential to be significantly wetter; in particular, having more summer rain. The glacial-transition (intermediate) climate is cooler than present-day and possibly significantly wetter, with relatively cool, dry summers and cool, wet winters. The glacial climates are even cooler and wetter. Each climate state has a range of possible behaviors, represented by bounding analog meteorological sites. Results for the range of net infiltration for each climate state are given in the next section.

Table I. Analog Sites for Climate States (Source: Ref. 2, Tables 3.2-1 and 3.2-5)

Climate State	Representative Meteorological Stations
Present-Day and Interglacial Climates	Yucca Mountain and vicinity
Monsoon Climate	Upper Bound: Nogales, Arizona Hobbs, New Mexico
	Lower Bound: Yucca Mountain and vicinity
Glacial-Transition (Intermediate) Climate	Upper Bound: Spokane, Rosalia, and St. John, Washington
	Lower Bound: Beowawe, Nevada Delta, Utah
Glacial Climates (three different glacial states are modeled)	Upper Bound: Lake Yellowstone, Wyoming One case also uses Browning and Simpson, Montana
	Lower Bound: Spokane, Rosalia, and St. John, Washington; or Browning and Simpson, Montana; or Simpson, Montana

INFILTRATION

Conceptual Model

Net infiltration is the penetration of water through the ground surface to a depth where it can no longer be withdrawn by evaporation or transpiration by plants. Infiltration occurs once water has entered bedrock or has penetrated below the root zone in soil. The conceptual model used for infiltration calculations is based on evidence from field studies at Yucca Mountain, combined with established concepts in soil physics and hydrology. The overall framework of the conceptual model is provided by the hydrologic cycle, including processes on the surface and just below the surface that affect net infiltration.

The main components of net infiltration are precipitation, evapotranspiration, and surface-water runoff and run-on. These components are incorporated into a watershed-scale, volume-balanced model using a snowpack submodel, an evaporation and net radiation submodel, one-dimensional (vertical) root-zone infiltration submodels, and a two-dimensional surface-water, flow-routing submodel (1, Section 3.5.2.4). Precipitation rate is provided by the analog meteorological stations discussed in the previous section and is spatially distributed based on an empirical precipitation–elevation relationship. Evapotranspiration is the combined process of evaporation and transpiration, which is the removal of moisture from soil by plants. The potential evapotranspiration is determined by an energy balance and is primarily dependent on net radiation, air temperature, ground heat flux, the saturation-specific humidity curve, and wind. Temperature is also spatially distributed for the model by using an empirical temperature–

elevation relationship. Net infiltration is modeled through soil layers of the root zone only. The change in root-zone water content is calculated as a daily change in water content, using a simple water-balance approach. The amount of daily net infiltration is limited by the bulk saturated hydraulic conductivity of the soil and storm duration. Water that exceeds the infiltration capacity of a soil column is routed to lower elevation nodes (runoff) for subsequent infiltration.

Considerable site information is available, including water-content profiles from 98 neutron moisture probes on Yucca Mountain from 1984 to 1995 and daily mean discharge for five stream gauges in operation at Yucca Mountain during 1994 and 1995 (6).

Implementation in the TSPA

Spatially distributed net infiltration rates were determined for each of the climate states using the infiltration process model. The model covers an area of 124 km^2 around Yucca Mountain, using a regular grid with 30-m spacing. The inputs to the model include daily precipitation and temperature; ground-surface elevation and geometry; parameters to describe surface water flow, soil type and depth; and bedrock type (6, Section 6.3.3).

For the upper-bound and lower-bound future climate states, daily precipitation and temperature data from the analog meteorological stations (Table I) were used directly. For present-day climate, data from Yucca Mountain and nearby meteorological stations were used. The present-day meteorological data were supplemented with a 100-year stochastic precipitation model because most of the records in the Yucca Mountain region go back less than 50 years (6, Section 6.9.2).

In addition to using different meteorological inputs, future-climate conditions are also represented by using different root-zone parameters to account for increases in vegetation density and changes in vegetation type for wetter and colder future climates (6, Section 6.9.4).

Treatment of Uncertainty and Variability

In the infiltration model, spatial variability is included by use of a two-dimensional model that incorporates the appropriate surface topography and geology. Temporal variability is included by using different infiltration simulations for different climate states; precipitation, temperature, and vegetation are varied with climate.

In order to represent infiltration uncertainty in TSPA simulations, three infiltration maps were generated for each climate state. They are termed the low-, medium-, and high-infiltration cases. For present-day climate, the medium-infiltration case was developed using the best estimates for precipitation, temperature, etc.; the high-infiltration case was developed by including precipitation data from one of the wetter nearby meteorological stations (on Rainier Mesa); and the low-infiltration case was developed by selectively choosing low infiltrations for each spatial location from a set of infiltration simulations. For future climates, the low-infiltration cases were simulated using the lower-bound climate analogs and the high-infiltration cases were simulated using the upper-bound climate analogs. The medium-infiltration cases were developed from the low- and high-infiltration maps by averaging them at each spatial location.

In order to include the three infiltration cases for each climate state into TSPA simulations, it is necessary to estimate their relative probability or likelihood. The probabilities were derived by means of a detailed analysis of infiltration uncertainty using the Monte Carlo method. The uncertainty analysis focused on 12 key input parameters, for which uncertainty distributions were developed. The key parameters include precipitation, bedrock and soil hydrologic properties, and potential evapotranspiration. The infiltration model was run 100 times, with each realization having different sampled values of the 12 key parameters. The glacial-transition (intermediate) climate was used for the analysis, because that climate state is in effect most of the time. Probabilities for the three infiltration cases were assigned in such a way as to make the log mean and standard deviation of the three-point discrete distribution (i.e., the distribution consisting of the three infiltration cases with defined probabilities) equal to the log mean and standard deviation of the distribution from the Monte Carlo simulation. Log values were used in deriving the weighting factors because the distribution has a more normal shape in log space than in linear space (1, Sections 3.5.2.6 and 3.5.3.2).

Results and Interpretation

Results of the infiltration modeling are summarized in Table II. The table shows computed average net infiltration over the repository area for the three infiltration cases for each climate state. In addition, the final column shows the estimated probabilities for the three infiltration cases. The infiltration numbers in Table II are plotted as time histories of repository-average net infiltration for the three infiltration cases in Figure 1. The results show the monsoon climate to have higher net infiltration than the present-day climate, which is expected because of the predicted higher precipitation rate. In addition, the glacial-transition climate is shown to have higher net infiltration than the monsoon climate, except for the low-infiltration case, and the glacial climates have higher net infiltration than the glacial-transition climate. The increase in net infiltration is a result of the colder temperatures, which reduce the amount of evapotranspiration. The glacial-transition low-infiltration case has lower infiltration than the monsoon low-infiltration case because of a more uniform seasonal distribution of precipitation. The average intensity and frequency of precipitation events for this case are not sufficient to overcome evapotranspiration from the root zone (6, Section 6.11.3).

Table II. Average Net Infiltrations and Probabilities for the Infiltration Cases (Source: Ref. 2, Tables 3.2-2 and 3.2-6)

Infiltration Case	Present-Day Climate	Monsoon Climate	Glacial-Transition Climate	Glacial Climates	Probability (All Climate States)
Low infiltration	0.4 mm/yr	4.7 mm/yr	2.2 mm/yr	17–37 mm/yr	17%
Medium infiltration	4.7 mm/yr	13 mm/yr	20 mm/yr	28–71 mm/yr	48%
High infiltration	12 mm/yr	20 mm/yr	37 mm/yr	71–110 mm/yr	35%

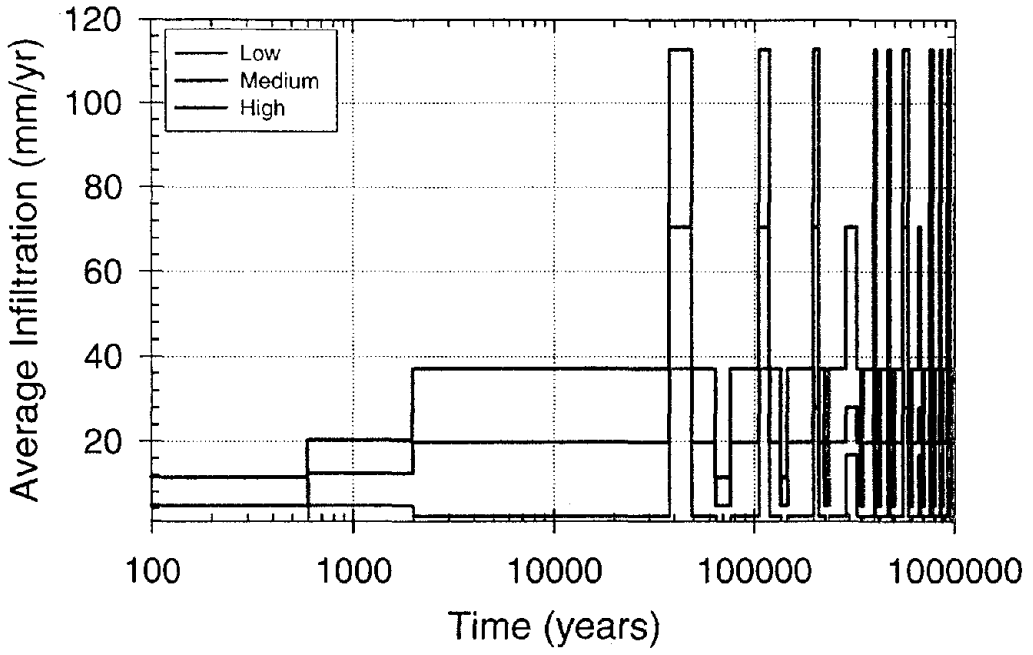

Fig. 1. Average net infiltration for the extended climate model (Source: Ref. 2, Figure 3.2-16).

MOUNTAIN-SCALE FLOW

Conceptual Model

UZ flow refers to the percolation of groundwater through rocks above the regional water table. UZ flow varies with the rock strata through which the water flows. The unsaturated zone at Yucca Mountain is composed of alternating layers of welded and nonwelded tuffs. The terms welded and nonwelded refer to the degree of consolidation of the rock when it was formed from volcanic ash millions of years ago. Welded tuff is hard, dense rock but is typically very fractured. The welded-tuff rock matrix is relatively impermeable, but the total permeability is high because of the fractures. Nonwelded tuff is softer and typically less fractured. Its matrix permeability is much higher than that of welded tuff matrix, but its total permeability is typically lower. A special case is zeolitic nonwelded tuff, which was altered during the original cooling in such a way that its matrix permeability is very low (similar to the matrix permeability of welded tuff). Zeolitic tuff may also have little fracturing, so that its total permeability is very low. Perched-water zones (localized saturated regions above the regional water table) have been observed above the zeolitic tuff in several boreholes, well below the potential repository elevation.

The mountain-scale UZ-flow model uses a dual-permeability conceptual flow model that captures the effects of fast flow paths and allows for weak fracture–matrix coupling. Flow is modeled in two interacting continua (fracture and matrix), with each continuum assigned its own spatially variable hydrologic properties, such as permeability and porosity. In general, the fractures are modeled as a highly permeable continuum having low porosity, while the matrix is modeled as a much less permeable continuum having higher porosity. Fracture–matrix

interaction is represented with an active-fracture model, in which only a portion of the fractures is actively flowing under unsaturated conditions (7). Major faults are included in the model explicitly. In fault zones, fracture density and permeability are higher than in the rest of the model, which enables them to act as preferential flow paths in parts of the model.

Wetter conditions in the past suggest that more groundwater flowed beneath Yucca Mountain than flows under modern conditions. Several studies have shown that the water table has risen at most 115 m in the past (8). For monsoon, glacial-transition, and glacial climates in the TSPA simulations, the water table is conservatively set to an elevation of 850 m above sea level, which is approximately 120 m higher than the present-day water table under the potential repository. Note that the potential repository is planned to be over 300 m above the present water table, so the potential repository would still be well above the water table, even with a rise of 120 m.

The mountain-scale UZ-flow model is a steady-state, isothermal model. Thermal effects can be neglected because flow is strongly perturbed by heat only near the emplacement drifts and at early times. Short-term episodic transients can be neglected because of the buffering effect of the Paintbrush nonwelded hydrogeologic unit above the potential repository. Long-term transients due to climate change are expected to be important to calculations of potential-repository performance, and those are included in the TSPA by approximating mountain-scale UZ flow with a sequence of steady states. With this approximation, the UZ flow fields can be calculated with the steady-state model and then the UZ-transport model can simply switch from one flow field to another at climate-change times.

Implementation in the TSPA

The three-dimensional, site-scale flow model for the unsaturated zone was used in calculating mountain-scale UZ flow for TSPA. Three-dimensional modeling is needed primarily because of flow characteristics below the potential repository, where significant lateral flow is believed to occur as a result of low-permeability zeolitic layers and perched water. The model uses the dual-permeability conceptual model, as mentioned previously.

The mountain-scale flow model is based on site data that include core measurements of porosity, permeability, saturation, and moisture potential; perched-water observations; fracture-frequency data from the ESF; air-pressure monitoring and air-permeability tests; and geochemical data. These data were used to estimate hydrologic parameters through direct calculations and calibration methods (1, Section 3.6). In addition, a geologic-framework model was used to define the proper stratigraphy for the UZ-flow model (1, Section 3.2).

UZ-flow calibration was done only for the present-day climate, because there is not sufficient information about paleohydrology to be able to calibrate flow for other climates. Thus, the flow for future climates is simulated using the same calibrated hydrologic properties and only changing the infiltration boundary condition at the surface. A total of 13 mountain-scale UZ flow fields are used in TSPA, nine for the base case and four additional ones for the extended climate definition.

Treatment of Uncertainty and Variability

In the UZ-flow model, spatial variability is included by use of a three-dimensional model that incorporates the appropriate geometry, geology, and hydrostratigraphy. Temporal variability is included by using different UZ-flow simulations for different climate states. The primary change in going from one climate to another is in the use of a different infiltration map for the upper boundary condition. In addition, the water table elevation is higher for future climates.

The uncertainty regarding the appropriate level of net infiltration, discussed previously, was carried forward through the mountain-scale flow model. Sensitivity analyses have shown that infiltration is the quantity that has the greatest impact on UZ flow and transport and that other uncertainties have little impact on repository performance (9). Although there is a considerable amount of data for calibrating the mountain-scale flow model, the hydrologic properties are not fully constrained, and it is possible to develop calibrated mountain-scale flow models for all three infiltration cases (1, Section 3.6).

Results and Interpretation

The average infiltrations in Table II also represent the average flux over the repository at the top boundary of the flow model. The probabilities for the three infiltration cases apply also to the UZ flow fields derived from those infiltration cases.

Figure 2 shows how the mountain-scale flow changes as it moves downward through the mountain. The figure shows the net infiltration flux that enters the top of the model at the ground surface (left), the percolation flux at the potential repository level (center), and the percolation flux that leaves the bottom of the model at the water table (right). The case pictured is medium infiltration for present-day climate. The model numerical mesh is superimposed for reference; the potential repository is located in the middle of the region, where there is a relatively uniform rectangular grid.

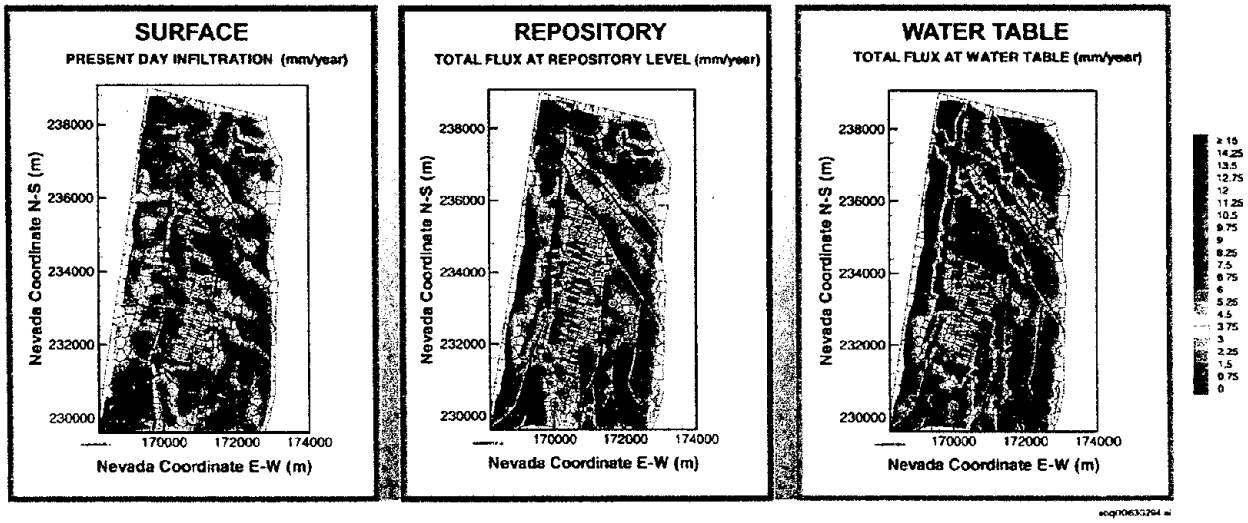

Fig. 2. Total percolation flux at three depths for present-day climate, medium-infiltration case (Source: Ref. 2, Figure 3.2-8).

Comparison of the three flux maps in Figure 2 shows that the simulated distribution of percolation flux at the potential repository level is similar to the distribution of net infiltration at the surface, but the distribution of percolation flux at the water table is quite different from the other two, indicating significant nonvertical flow between the potential repository and the water table. The high-infiltration band along the crest of the mountain in the left-hand map is somewhat spread out by the time it arrives at the potential repository (center map), and a portion of the flow has been diverted down the Solitario Canyon fault. Similarly, there is significant flow down the other faults as well. At the water table (right-hand map), much of the water is flowing down the faults, more so in the north than in the south. The fraction of total flow that is in the faults over the entire model domain increases from 4 percent at the ground surface to 15 percent at the potential repository level to 35 percent at the water table (1, Table 3.7-3). The diversion of water into flow down faults is much less strong in the southern half of the model domain. There, the fraction of flow in faults increases from 4 percent at the ground surface to 20 percent at the potential repository level and then decreases slightly to 16 percent at the water table (1, Table 3.7-3). The difference in behavior between the northern and southern parts of the model domain occurs because the Calico Hills nonwelded tuff is largely zeolitized in the north, resulting in a low-permeability zone and extensive perched water, which causes strong lateral diversion to more permeable fault zones in the simulation.

SEEPAGE INTO DRIFTS

Conceptual Model

Seepage is the movement of liquid water into emplacement drifts. The basic conceptual model for seepage is that openings in unsaturated media act as capillary barriers and divert water around them. This capillary-barrier effect has been tested in the potential repository host rock at Yucca Mountain in the Exploratory Studies Facility (ESF) by seepage tests in which water is injected above a niche (a side tunnel off the main tunnel). Results from the tests indicate that most of the water does not seep into an opening less than 1 m below the water-release point. In addition, no naturally occurring and continuous seeps have been observed so far in the ESF, although the lack of seeps may be partially caused by drying from tunnel ventilation.

Important factors affecting drift seepage include heterogeneity on the drift scale, flow channeling on larger scales (possible focusing of flow above drifts), fracture permeability and capillarity, drift geometry and its degradation over time, the excavation-disturbed zone around the drifts, and the thermal perturbation caused by emplacement of waste. The excavation-disturbed zone (EDZ) refers to the region around an excavation where fracture properties are changed from their pre-excavation values. Generally, fractures open up somewhat in the EDZ, and the rock may be broken to create new fractures as well. One result is that fracture permeability is increased significantly in this zone.

As with the modeling of mountain-scale flow, the dual-permeability model would be preferred for modeling seepage at the drift scale. However, to simplify the drift-scale calculations, effects of the rock matrix were not considered, and flow was calculated using a model for only the fracture continuum. This simplification is conservative compared to the dual-permeability model, because the effect of including the matrix would be to decrease the fracture flow and

reduce the amount of seepage. (The large capillary suction in matrix pores prevents matrix flow from seeping into drift openings.)

Implementation in the TSPA

Modeling of seepage into drifts was done in three steps:

1. Conceptual models were tested against data from the niche seepage tests, and calibrated properties were derived (1, Section 3.9.4; 10). Fracture permeability is measured by means of air-injection tests, but capillarity cannot be measured directly. Calibrating the three-dimensional, heterogeneous seepage process model against seepage tests produces values for the fracture capillarity that implicitly include discrete-fracture effects and effects of the EDZ around the niche.

2. Because of uncertainty and spatial variability in percolation flux and fracture hydrologic parameters, the seepage process model was run for a wide range of parameter inputs (1, Section 3.9.5; 11). Also, several other effects were evaluated, including changes in drift shape due to rockfall and possible correlation between fracture permeability and capillarity.

3. A probabilistic seepage-abstraction model was developed using the results of the simulations from step 2, including adjustments to account for drift degradation, possible preferential paths provided by degraded rock bolts, possible correlation between fracture permeability and capillarity, and channeling of flow above the drifts (1, Section 3.9.6; 12).

Treatment of Uncertainty and Variability

Within the TSPA model, seepage is parameterized by four quantities: the seepage fraction (fraction of waste-package locations that have seepage), the mean seep flow rate for locations with seepage, the standard deviation of seep flow rate for locations with seepage, and a flow-focusing factor that represents effects of flow channeling (because only a subset of fractures are actively flowing). Uncertainty distributions were developed for these four quantities, and values were sampled from the uncertainty distributions for each realization (see Table III). There have been two major sets of TSPA simulations recently, and the models used are referred to as the base-case TSPA model (2) and the supplemental TSPA model (4). As noted in the table, there are several differences in the seepage treatment between the two. The differences reflect additional data collection and additional seepage modeling studies between the times of the two TSPAs. In addition to changes in the four parameters mentioned above, an additional parameter was introduced in the supplemental TSPA model, to include the possibility of episodic flow. The episodicity factor represents the fraction of time that episodic flow occurs.

The distributions for the first three parameters in Table III were developed by using air-permeability data and seepage-test data to define distributions for the uncertainty and spatial variability of permeability and capillarity. Those distributions were combined with seepage modeling results to obtain uncertainty and spatial-variability distributions for seepage as a function of percolation flux. The flow-focusing distributions for the TSPA base case were based on estimates of spacing of actively flowing fractures in the mountain-scale flow model, while the distribution for the supplemental TSPA model was based on mountain-scale flow simulations with heterogeneous permeability. The episodicity distribution was based on a conceptual model

for episodic flow caused by accumulation of water at fracture asperities followed by drainage after buildup of sufficient water pressure.

The percolation flux for input to the seepage-abstraction model is taken from thermal-hydrology calculations in order to approximate thermal perturbations to seepage. For the TSPA simulations, thermally perturbed percolation histories were calculated for several hundred repository locations using the multiscale thermal-hydrology model (13). However, engineered-system calculations within the TSPA model are based on a much smaller number of environmental groups (2, Section 3.3.2). Quantities such as temperature and relative humidity are averaged over those groups for use by most of the engineered-system models. Because of the nonlinear relationship between seepage and percolation flux, seepage histories are generated for all the locations in each environmental group and then averaged for use by the other models, rather than averaging the percolation flux and calculating seepage from the averaged percolation history.

Table III. Uncertainty Distributions Used to Represent Seepage

Parameter	Distribution Type
Seepage fraction (fraction of locations with seepage)	Triangular. Minimum, most likely, and maximum are functions of percolation flux. Different functions for TSPA base case and supplemental TSPA model.
Mean seep flow rate for locations with seepage	Triangular. Minimum, most likely, and maximum are functions of percolation flux. Different functions for TSPA base case and supplemental TSPA model.
Standard deviation of seep flow rate for locations with seepage	Triangular. Minimum, most likely, and maximum are functions of percolation flux. Different functions for TSPA base case and supplemental TSPA model.
Flow-focusing factor (factor by which flow is increased at locations where flow is focused; flow is decreased at other locations to compensate)	TSPA base case: Log-uniform with minimum of 1 and maximum of 9.7–47, depending on the infiltration case. Supplemental TSPA model: Exponential with minimum of 1 and mean of 2.
Episodicity factor (fraction of time that flow occurs)	TSPA base case: Set to 1 (i.e., no episodic flow). Supplemental TSPA model: Log-uniform with minimum of 10^{-4} and maximum of 1.

NOTE: Distributions for TSPA base case are described in Ref. 2, Section 3.2.4
Distributions for supplemental TSPA model are described in Ref. 4, Section 3.2.2

Results and Interpretation

An example of TSPA seepage results is given in Figure 3, which shows the mean seep flow rate in one of the environmental groups for the TSPA base case and for two sub-cases of the supplemental TSPA model. The environmental group presented is the one that has the greatest number of waste packages of all groups that have seepage. Several features of the models can be seen in the figure:

- The many spikes after 10,000 years in the supplemental TSPA model occur because the supplemental model uses the extended climate definition, discussed earlier. Seepage is higher during glacial climates and lower during interglacial climates.

- For the intermediate climate, which is in effect most of the time after 2000 years, the mean seep flow rate is lower in the supplemental TSPA model than in the TSPA base case. This reduction is primarily because the supplemental model includes less flow focusing (see Table III). Associated with that change is one that cannot be seen in the figure: The fraction of waste packages that have seepage is higher in the supplemental TSPA model than in the TSPA base case.

- The large differences during the first few hundred years result from differences in the way thermal effects on seepage are incorporated. In the TSPA base case, no credit is taken for seepage reduction due to evaporation and imbibition of water percolating through the hot, dry near-field rock during the thermal pulse. As a result of the particular way in which the thermal effects are implemented, in the base-case model the amount of seepage is actually higher during the hottest period. The supplemental TSPA model has a somewhat more realistic treatment of thermal effects, so seepage is suppressed during the hot period, especially in the higher-temperature case.

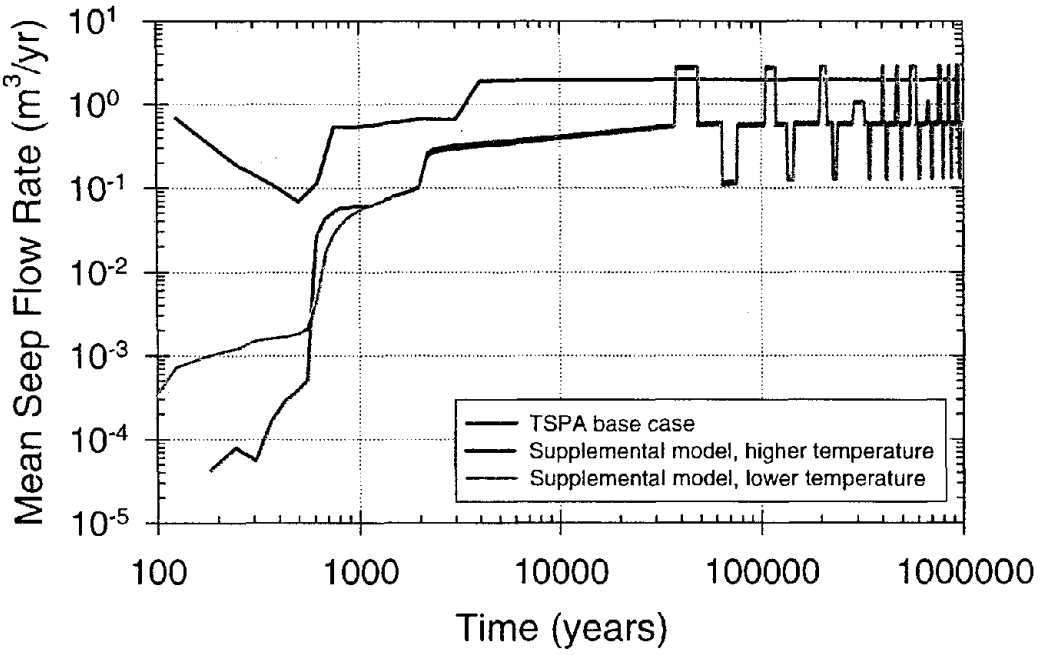

Fig. 3. Comparison of mean seep flow rate for waste packages with commercial spent nuclear fuel in locations where infiltration is 20–60 mm/yr (Source: Ref. 4, Figure 4.2-5).

RADIONUCLIDE TRANSPORT

Conceptual Model

Radionuclides can migrate in groundwater as dissolved molecular species or by being associated with colloids. Five basic processes affect the movement of dissolved or colloidal radionuclides: advection, diffusion, sorption, hydrodynamic dispersion, and radioactive decay. Sorption is potentially important because it slows, or retards, the transport of radionuclides. Diffusion of

radionuclides out of fractures into matrix pores is also a potential retardation mechanism because matrix transport is generally slower than fracture transport. However, sorption and matrix diffusion have less effect on colloids, so radionuclides can be more mobile on colloids than if dissolved in the water. One aspect of potential significance with respect to chain decay is that daughter products may have significantly different sorption behavior than the parent radionuclide, thus affecting transport as a function of time.

As discussed previously, a dual-permeability model is used to represent mountain-scale UZ flow. The same concept is used to model radionuclide transport—a dual-continuum model, in which fractures and matrix are distinct interacting continua that coexist at every point in the modeling domain. Each continuum is assigned its own transport properties in addition to having its own hydrologic properties. The properties can vary spatially among hydrogeologic units.

Since mountain-scale UZ flow is represented as a sequence of steady states, the flow field is changed abruptly from one to another at the time of a climate change. The transport calculation then continues with the new flow field. In addition to the change in the flow field, the location of the water table can also be changed abruptly at the time of climate change. When the water table rises with a climate change, the radionuclides in the UZ between the previous and new water-table elevations are immediately moved to the saturated zone.

Colloids, because they are small solids (from 1 nm to 10 μm), can interact with radionuclides through sorption mechanisms. Unlike sorption of radionuclides to the immobile rock matrix, however, radionuclides sorbed on colloids are potentially mobile. Therefore, colloids can facilitate radionuclide transport at a faster rate. Another form of colloidal radionuclide movement occurs when the radionuclide is an integral component of the colloid structure. In this case, the radionuclide is irreversibly bound to the colloid, as compared to the reversible sorption mechanism. These two types of colloids will be referred to as reversible and irreversible colloids, respectively.

For reversible colloids, radionuclides sorbed to colloids are assumed to be in equilibrium with radionuclides in solution. The ratio of the concentration of a radionuclide sorbed on colloids to the concentration in solution is represented by a parameter called K_c (14, Section 5.3). The K_c ratio is a function of the concentration of colloids and the sorption coefficient for the given radionuclide onto the given type of colloid. Because the radionuclides on reversible colloids are in equilibrium with radionuclides in solution, matrix diffusion can cause some effective slowing of the transport even though the colloids themselves do not diffuse into the matrix. (Diffusion of dissolved radionuclides into the matrix reduces the concentration in the fractures, which reduces the amount of radionuclides sorbed to the colloids and, thus, effectively slows the transport.)

Implementation in the TSPA

Radionuclide transport in the UZ is implemented by using the residence-time transfer-function particle-tracking technique (1, Section 3.11.13.3; 14). This technique is a cell-based approach in which particles move from cell to cell in a numerical grid. Particle locations within cells are not tracked, as they are in some particle-tracking techniques, but, rather, movement from cell to cell is computed probabilistically, based on transfer functions. The transfer functions are defined

using analytical or semianalytical solutions of the transport equations, and represent probability distributions of the residence time (the amount of time that a particle resides in a cell).

Releases from the engineered-barrier system (EBS) are computed for a limited number of environmental groups, which are based on infiltration, waste type, and seepage condition (2, Section 3.3.2). Since infiltration is important for UZ transport as well, radionuclides are released into the UZ at locations consistent with the environmental group from which they are released. Each environmental group is associated with one of five infiltration bins, based on the infiltration at each spatial location during the glacial-transition climate. The ranges for the bins are 0–3 mm/yr, 3–10 mm/yr, 10–20 mm/yr, 20–60 mm/yr, and 60+ mm/yr.

In order to avoid spreading out the radionuclides artificially, the release of radionuclides into the unsaturated zone takes into account the number of waste packages that have failed within each of the five infiltration bins. If only one waste package has failed in a bin, the releases for that bin are put into a single UZ cell, sampled randomly from the cells in that bin. If two waste packages have failed, then releases are put into two randomly selected cells. This process continues for additional waste packages until the number of failed waste packages is equal to the number of cells in the bin. At that point, the releases are spread over all cells in the bin, and additional waste package failures cause no change to the release locations. Artificial spread of radionuclides in the UZ is further reduced by gathering the releases from the UZ into a few discrete locations at the water table for input to the saturated-zone-transport model.

In the base-case TSPA model, radionuclides are released from the EBS into the fracture continuum of the UZ-transport model, so radionuclide transport through the UZ is initially through fractures. In order to make the model a little more realistic in the supplemental TSPA, radionuclides that advect out of the EBS are still released into the UZ fracture continuum, but radionuclides that diffuse out of the EBS are released into the UZ matrix continuum. Neither model accounts for the fact that there is expected to be a flux "shadow" below the drifts because flow tends to divert around open drifts, resulting in reduced flow in the region immediately below an emplacement drift. Neglecting the flux "shadow" below the drift is conservative because the drier conditions at the EBS–UZ interface would increase transport times if included.

Treatment of Uncertainty and Variability

In the UZ-transport model, spatial variability is included by use of a three-dimensional model that incorporates the appropriate geometry and geology. Temporal variability is included by using different UZ flow fields for different climate states. None of the other transport properties changes with time. Of course, the radionuclide source term also varies with time.

Uncertainty is included in the UZ-transport model by defining uncertainty distributions for a number of input parameters. Values of these parameters for each TSPA realization are sampled from the distributions. Thus, each realization of the total system has a unique set of input parameters, each of which is within the range that is considered to be defensible.

Some of the uncertainty in UZ-transport results from uncertainties passed to it by other models: uncertainty in infiltration and UZ flow from the UZ-flow model; uncertainty in the number of failed waste packages from the waste-package-degradation model; and uncertainty in numerous

EBS parameters and processes in the radionuclide source term received from the EBS-transport model. The uncertainty distributions for parameters of the UZ-transport model itself are summarized in Tables IV and V. Some key parameters that are treated as certain in the TSPA (i.e., that have single values rather than uncertainty distributions) are also listed.

Table IV. Sorption Coefficients for UZ Transport (Source: Ref. 2, Table 3.7-1)

Parameter Description	Distribution
K_d for Am and Th in devitrified tuff (mL/g)	Uniform; min = 100, max = 2,000
K_d for Am and Th in vitric tuff (mL/g)	Beta; mean = 400, COV = 0.2, min = 100, max = 1,000
K_d for Am and Th in zeolitic tuff (mL/g)	Uniform; min = 100, max =1,000
K_d for Pu in devitrified tuff (mL/g)	Uniform; min = 5, max = 70
K_d for Pu in vitric and zeolitic tuff (mL/g)	Beta; mean = 100, COV = 0.25, min = 30, max = 200
K_d for Np in devitrified tuff (mL/g)	Beta; mean = 0.3, COV = 0.3, min = 0, max = 1
K_d for Np in vitric tuff (mL/g)	Beta; mean =0.3, COV = 1, min = 0, max = 1
K_d for Np in zeolitic tuff (mL/g)	Beta; mean = 0.5, COV = 0.25, min = 0, max = 3
K_d for U in devitrified tuff (mL/g)	Beta; mean = 0.5, COV = 0.3, min = 0, max = 2
K_d for U in vitric tuff (mL/g)	Beta; mean = 0.5, COV = 0.3, min = 0, max = 1
K_d for U in zeolitic tuff (mL/g)	Beta; mean = 4, COV = 1, min = 0, max = 10
K_d for Pa in all units (mL/g)	Uniform; min = 0, max = 100
K_d for I, Tc, and C in all units (mL/g)	Not sampled; 0

NOTE: COV = coefficient of variation = standard deviation divided by mean

Table V. Additional Key Transport Parameters (Source: Ref. 2, Table 3.7-2)

Parameter Description	Distribution
Diffusion Coefficient for Am, Pu, Np, U, Pa, Th (m^2/s)	Beta; mean = 1.6×10^{-10}, SD = 0.5×10^{-10}, min = 0, max = 10^{-9}
Diffusion Coefficient for I, Tc, C (m^2/s)	Beta; mean = 3.2×10^{-11}, SD = 10^{-11}, min = 0, max = 10^{-9}
Dispersivity for both fractures and matrix (m)	Not sampled; 20
Fracture aperture (mm)	Log-normal; geometric mean is different for each hydrogeologic unit, varying from 1.5 to 4.6 outside of fault zones and from 6.8 to 8.4 in fault zones; geometric SD = 1.9
Fracture spacing (m)	Not sampled; different for each hydrogeologic unit, varying from 0.23 to 25 outside of fault zones and from 0.59 to 7.7 in fault zones
Colloid partitioning factor (K_c)	Log-normal; geometric mean = 3×10^{-3}, geometric SD = 10; only used for reversible colloids
Colloid retardation factor	Not sampled; 1
Colloid size distribution (nm)	Not sampled; distribution of sizes from 1 to 450, median size approximately 75; only used for irreversible colloids
Fraction of colloids that can enter one matrix unit from another	Not sampled; function of colloid size and hydrogeologic unit; only used for irreversible colloids
Fraction of colloids that can enter the matrix from fractures	Not sampled; different for each hydrogeologic unit, varying from 4% to 79%; only used for irreversible colloids

NOTE: SD = standard deviation (geometric SD is 10 raised to the power equal to the standard deviation of the logs)

Results and Interpretation

An example of UZ radionuclide-transport times is given in Figure 4. The base-case TSPA model was used to generate this figure, including all the parameter uncertainty distributions shown in Tables IV and V. One hundred realizations were simulated, with each realization having a different set of transport parameters, sampled from the uncertainty distributions. In each realization, a pulse of radionuclides was released at time zero, spread uniformly over the potential repository area. The curves shown in the figure are the average breakthrough curves over all 100 realizations. Some realizations have faster than average transport, and others have slower than average transport. Results are shown for technetium and neptunium, and plutonium transport results are shown for the two types of colloid-facilitated transport: reversible and irreversible attachment to colloids. These simulations include the climate changes at 600 and 2000 years. The transport behavior clearly changes at 600 years because of the change from present-day to monsoon climate. A small change in slope is also observable at 2000 years (when the climate changes from monsoon to glacial-transition).

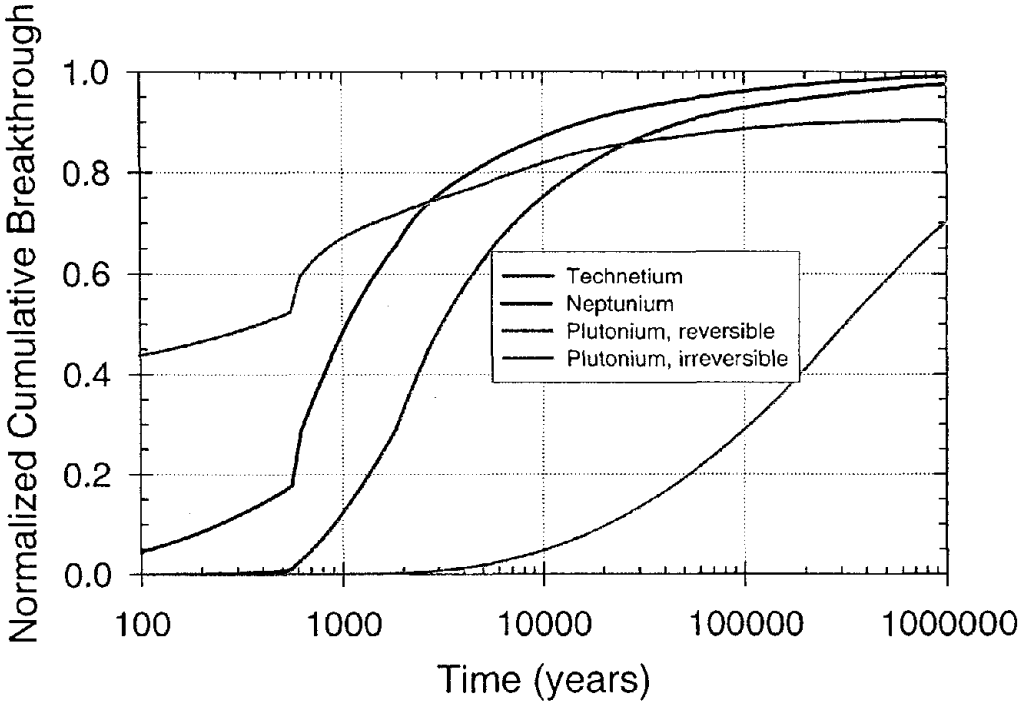

Fig. 4. Mean breakthrough curves at the water table for the base-case TSPA model (Source: Ref. 2, Figure 3.7-12).

It can be seen in Figure 4 that the irreversible colloids have the fastest transport in the model, with 50 percent of the irreversible colloids reaching the water table in about 500 years. The effects of physical filtration are noticeable, as the breakthrough curve for irreversible colloids levels off at a normalized breakthrough of about 90 percent. This occurs because approximately 10 percent of the irreversible colloids have been trapped at unit interfaces (on average). In comparison, the reversible colloids have the slowest transport in the model, taking about 300,000 years to reach a 50 percent breakthrough. And only 70 percent of the reversible colloids reach the water table within 1 million years. Technetium reaches 50 percent breakthrough in a little

over 1,000 years, and neptunium reaches 50 percent breakthrough in about 3,000 years, with some particles taking much longer for both.

ACKNOWLEDGMENTS

This work was supported by the Yucca Mountain Site Characterization Office as part of the Civilian Radioactive Waste Management Program, which is managed by the U.S. Department of Energy, Yucca Mountain Site Characterization Project. Sandia is a multiprogram laboratory operated by Sandia Corporation, a Lockheed Martin Company, for the United States Department of Energy under Contract DE-AC04-94-AL85000.

REFERENCES

1. *Unsaturated Zone Flow and Transport Model Process Model Report*, Civilian Radioactive Waste Management System Management and Operating Contractor (CRWMS M&O) report TDR-NBS-HS-000002 REV 00 ICN 02 (2000).
2. *Total System Performance Assessment for the Site Recommendation*, CRWMS M&O report TDR-WIS-PA-000001 REV 00 ICN 01 (2000).
3. *FY01 Supplemental Science and Performance Analyses, Volume 1: Scientific Bases and Analyses*, Bechtel SAIC Company report TDR-MGR-MD-000007 REV 00 ICN 01 (2001).
4. *FY01 Supplemental Science and Performance Analyses, Volume 2: Performance Analyses*, Bechtel SAIC Company report TDR-MGR-PA-000001 REV 00 (2001).
5. R. M. FORESTER, *Future Climate Analysis*, CRWMS M&O report ANL-NBS-GS-000008 REV 00 (2000).
6. J. A. HEVESI, *Simulation of Net Infiltration for Modern and Potential Future Climates*, CRWMS M&O report ANL-NBS-HS-000032 REV 00 ICN 01 (2000).
7. H. H. LIU, C. DOUGHTY, and G. S. BODVARSSON, "An Active Fracture Model for Unsaturated Flow and Transport in Fractured Rocks," *Water Resources Research* **34** (10), 2633–2646 (1998)
8. C. K. HO, *Abstraction of Flow Fields for TSPA*, CRWMS M&O report ANL-NBS-HS-000023 REV 00 ICN 01, Section 6.2 (2000).
9. *Viability Assessment of a Repository at Yucca Mountain, Volume 3: Total System Performance Assessment*, U. S. Department of Energy report DOE/RW-0508/V3, Section 5.1.3 (1998).
10. S. FINSTERLE, C. F. AHLERS, and R. C. TRAUTZ, *Seepage Calibration Model and Seepage Testing Data*, CRWMS M&O report MDL-NBS-HS-000004 REV 01 (2000).
11. G. LI and C.-F. TSANG, *Seepage Model for PA Including Drift Collapse*, CRWMS M&O report MDL-NBS-HS-000002 REV 01 (2000).
12. M. L. WILSON, *Abstraction of Drift Seepage*, CRWMS M&O report ANL-NBS-MD-000005 REV 01 (2001).
13. T. BUSCHECK, *Multiscale Thermohydologic Model*, CRWMS M&O report ANL-EBS-MD-000049 REV 00 ICN 01 (2000).
14. B. ROBINSON, *Particle Tracking Model and Abstraction of Transport Processes*, CRWMS M&O report ANL-NBS-HS-000026 REV 00 (2000).

NOTE: Yucca Mountain Project reports are available from the Yucca Mountain Project (see http://www.ymp.gov/doclist.htm).